



Femtosecond laser-matter interactions in ternary zinc phosphate glasses

J. HERNANDEZ-RUEDA,^{1,2,*} N. W. TROY,¹ P. FREUDENBERGER,³ R. K. BROW,³ AND D. M. KROL^{1,2}

¹Department of Materials Science and Engineering, University of California Davis, CA 95616, USA

²Debye Institute for Nanomaterials Science, Utrecht University, P. O. Box 80000, 3508 TA Utrecht, The Netherlands

³Missouri University of Science and Technology, Rolla, MO 65409, USA

*fjavahr@gmail.com

Abstract: We investigate the interaction of ultrashort laser pulses with ternary zinc phosphate glasses. We explore the viability of ten different glass compositions with different levels of alumina to inscribe optical waveguides via the fs-laser direct writing technique, finding that only samples with [O]/[P] ratios of 3.25 are suitable candidates. We also test a zinc magnesium phosphate glass to fabricate waveguide Bragg gratings in order to generate filters and mirrors with specific spectral properties. Confocal Raman spectroscopy inspection shows that laser-damaged material exhibits a relative intensity decrease and a subtle blue-shift on the 1209 cm^{-1} Raman peak, which implies a relative reduction on the content of $Q^{(2)}$ tetrahedra species within the glass network thus suggesting a laser-induced depolymerization. In contrast, optical waveguides and smooth laser-induced changes do not exhibit such noticeable structural modifications.

© 2018 Optical Society of America under the terms of the [OSA Open Access Publishing Agreement](#)

1. Introduction

The use of ultrashort laser sources for a variety of scientific, medical and technological applications is continuously increasing [1–5]. Over the last two decades, femtosecond laser micromachining inside transparent materials has attracted much attention [6–19]. Both pulse shaping and spatial beam shaping are currently broadly investigated in order to improve, control and achieve a better understanding of ultrafast laser materials processing [20–26]. In particular, the use of slit shaping is becoming a standard complementary technique to femtosecond laser waveguide writing inside transparent materials [20, 21]. Furthermore, the use of high repetition rate lasers allows researchers to exploit heat accumulation effects in order to inscribe low-loss optical waveguides [4, 21, 27, 28]. These heat accumulation effects have been proven to be extremely interesting to generate photonic devices by controlling the ultrafast laser-driven ion migration in glasses [29, 30]. In addition to the rapid development of advanced laser materials processing techniques, the study of the role of the material composition and properties in this context is gaining importance. For instance, phosphate glasses are ideal host materials for the fabrication of active devices because they can incorporate high concentrations of rare-earth ions [31, 32]. Many commercially available phosphate glasses have been tested exhibiting both negative and positive index changes under fs-laser waveguide writing [28, 33–35].

We have recently found that fs-laser writing in binary zinc polyphosphate glasses yields good quality waveguides for compositions with [O]/[P] ratios close to 3.25 [32, 36–38]. For practical applications multicomponent glasses offer more robust stability as well as better corrosion resistance. In order to determine if an [O]/[P] ratio of 3.25 is also required in such glasses we investigate femtosecond laser waveguide fabrication in a series of zinc aluminium phosphate glasses with [O]/[P] ratios varying between 3.00 and 3.50. We first study the effect of the content of alumina in ternary glasses. We additionally test the influence of the pulse duration, in order to reduce undesired non-linear effects during laser processing as well as premature laser damage.

Subsequently, we show that zinc magnesium phosphate glasses doped with rare earth ions are suitable for fs-laser fabrication of filters and mirrors by inscribing waveguide Bragg gratings. Finally, we discuss the fs-laser induced structural changes by using Raman confocal spectroscopy.

2. Experimental methods

2.1. Waveguide writing and characterization

We carried out the fabrication of tracks of modified glass using femtosecond laser writing [39]. This technique consists of optically inscribing patterns by tightly focusing a fs-laser pulse (≈ 100 fs) inside a transparent target, whose position and movement is precisely controlled. In this scenario, the laser-glass interaction becomes extremely non-linear resulting in permanent modification of the irradiated material around the focal volume. Initially, the fs-laser pulse drives the formation of a dense electron plasma (typically 10^{19} - 10^{21} cm $^{-3}$). The laser-matter interaction is mediated by strong field ionization, which includes multi-photon ionization and tunneling ionization and depends on the magnitude of the electric field strength. Subsequently, seed electrons absorb photons via inverse bremsstrahlung, gaining energy and leading to impact ionization and avalanche ionization, which in turn increase the density of electrons in the conduction band. Once the laser pulse is no longer present, the electron plasma relaxation and the energy transfer to the lattice follow. The modifications of the glass structure induced by the transfer of energy largely depend on the laser-processing parameters (wavelength, duration, pulse energy, writing speed, repetition rate, focusing conditions) as well as on the material parameters (composition, thermal properties, etc.).

In this work, we used a femtosecond laser amplifier (Merlin-Spitfire LCX, Spectra Physics) that generates a 1 kHz train of Fourier limited pulses of ≈ 200 fs pulse duration at a wavelength of 800 nm. The pulse duration can be stretched by adjusting the compression stage of the amplifier and characterized using a single shot autocorrelator (SSA Spectra Physics). Fig. 1 shows a schematic of the experimental setup employed to inscribe optical waveguides, tracks of modified material and waveguide Bragg gratings inside our set of ternary phosphate glass samples. We controlled the laser energy delivered inside the sample by using a lambda half wave-plate combined with a polarizing beam cube. Once the energy per pulse was reduced to be equal or less than 10 μ J, we used a confocal system to clean the spatial profile of the laser, which uses two lenses with a $f = 500$ mm and a pinhole with a diameter of 150 μ m. After that, the laser beam was focused inside the glass sample by employing a long working distance microscope objective with a numerical aperture of 0.25, which leads to a beam waist of $w_0 = 3.9$ μ m. The sample was attached to an Aerotech air bearing stage that translated it along the laser propagation axis at a speed of 50 μ m/s. Note that the polarization direction is perpendicular to the writing direction. In addition the glass sample was sitting on a 5D holder that allowed us to control its precise position along three orthogonal axes and two relevant angles, which are particularly sensitive for measuring the waveguide operation. We monitored the waveguide fabrication using an in situ microscope, that also served to inspect the input cross section and the lateral view of the inscribed lines. After laser processing, we used a continuous wave laser (660 nm) to check waveguiding operation by measuring the far and near field output modes. We coupled the beam into the input facet of the waveguides and imaged their output end using another lens objective (NA= 0.22, 10x) and an imaging system (tube lens and CCD camera). We additionally measured the numerical aperture of the far field output cone in order to characterize the laser-induced refractive index change.

Waveguide Bragg-grating inscription was carried out using the same experimental setup with a Nikon 50x/0.55 microscope objective (CFI 60 LU PLAN). We translated the sample transversely with respect to the laser beam propagation axis at different processing speeds in order to control the grating index periodicity. We made use of a 400 μ m slit to create circular modifications at a writing depth of 250 μ m [20,40]. After laser processing, the sample front and back surfaces were

ground and polished in order to place the waveguides at the surface for better coupling results. The length of the waveguides after polishing the sample was measured to be 4 mm.

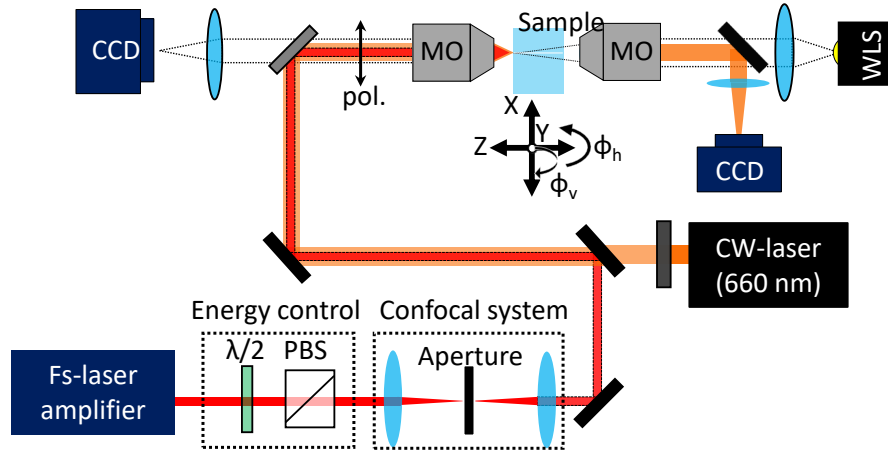


Fig. 1. Experimental setup for waveguide writing, frontal and lateral optical microscopy inspection and near field characterization.

2.2. Glass sample preparation

We study fs-laser direct-writing inside zinc aluminum phosphate glasses with ten compositions. The glass specimens were prepared by mixing reagent grade Al_2O_3 , ZnO , and $\text{NH}_4\text{H}_2\text{PO}_4$ that were calcined at 500°C for 12 hours in alumina crucibles. Afterwards, they were melted at 1100°C for 2 hours and subsequently quenched to form a glass frit. The glass was ground with a mortar and remelted in a platinum crucible for 1 hour at 1100°C . The melts were then poured in steel molds, cooled and annealed near the glass transition temperature. An additional glass sample including magnesium and rare earths was prepared following the same procedure, but employing reagent grade ZnO , MgO , Er_2O_3 , Yb_2O_3 and $\text{NH}_4\text{H}_2\text{PO}_4$ in the raw mixture.

We polished the surface of the samples to a flatness better than a $\lambda/5$. The overall surface flatness was characterized using a Zygo interferometer. The samples presented excellent optical quality, with no bubbles or striations, making them ideal for waveguide inscription. Finally, we cleaned the samples before and after fs-laser processing by using organic solvents.

To characterize the composition of the glasses, we used energy dispersive spectroscopy (EDS) within a scanning electron microscope (SEM, Helios NanoLab 600), obtaining compositions that are well within the expected tolerances. The levels of ZnO , P_2O_5 and alumina, along with the $[\text{O}]/[\text{P}]$ ratio of representative samples are specified in Table 1. The Er-Yb doped zinc magnesium phosphate glass sample composition is 28 % MgO , 28 % ZnO , 42 % P_2O_5 , 1.3 % Yb_2O_3 and 0.7 % Er_2O_3 (mole %). We observe that the SEM data indicate slight discrepancies ($< 1.5\%$) in the concentration of alumina when compared to the initial raw mixtures, which is likely due to the use of alumina crucibles, and this amount of alumina into the glass is to be expected. The $[\text{O}]/[\text{P}]$ ratios obtained from the EDS measurements of representative samples, which we include in Table 1, illustrate good agreement with the batched ratios.

Table 1. Zinc alumina phosphate glass sample compositions (mole %), [O]/[P] ratios (with the EDS analyzed ratio in parenthesis), waveguide operation, refractive index change and waveguiding upper threshold. These samples are used to study optical waveguiding suitability.

Composition

ZnO	P ₂ O ₅	Al ₂ O ₃	[O]/[P] ratio (EDS)	Waveguiding	Δn	Upper threshold
50	50	0	3.00 (–)	No		
40	55	5	3.00 (3.04)	No		
30	60	10	3.00 (–)	No		
40	50	10	3.20 (3.18)	No		
60	40	0	3.25 (3.24)	Yes	3×10^{-4}	1.50 μJ
51	44	5	3.25 (3.25)	Yes	2×10^{-4}	0.75 μJ
42	48	10	3.25 (3.24)	Yes	3×10^{-4}	0.50 μJ
45	45	10	3.33 (3.33)	No		
65	35	0	3.43 (–)	No		
50	40	10	3.50 (3.48)	No		

3. Results

3.1. Femtosecond laser waveguide writing in zinc aluminum phosphate glasses

Using our experimental setup, we inscribed a variety of tracks of modified material inside glass samples with several compositions (Table 1). A set of laser-induced modifications were systematically made with pulse energies ranging from 0.25 μJ to 10.00 μJ and two different pulse durations (200 fs and 400 fs). We observe three different outcomes, namely unmodified material when using sub-threshold laser energies ($E < E_{th}^s$), tracks with smooth optical changes ($E_{th}^s \leq E < E_{th}^d$) and tracks of damaged material when using higher energies ($E \geq E_{th}^d$). We illustrate the last two in Fig. 2, where white light microscopy images show the input facet and lateral view of lines inscribed inside the glass sample with a 5 % Al₂O₃, 51 % ZnO and 44 % P₂O₅ composition. The images present bright and dark round regions of the cross section of the laser modified material and lateral views that show tracks with a smooth (left) and heterogeneous (center) appearance. Microscopy images of the input facet that present a bright and circular shape are usually good candidates for waveguiding operation. That, we confirm by measuring the near field profile of the guided light using a CW-laser at 660 nm, as shown within the inset on the leftmost image. The profile illustrates Airy rings due to the interference and diffraction of the guided light caused by a numerical aperture mismatch. In contrast, a black and circular cross section is indicative of a track of damage. The track shown in the center was checked not to guide light. The image on the right illustrates two parallel tracks of modified material that cannot guide light individually but when machined next to each other they result in a waveguide (see guided mode profile), where guiding takes place in the region between the damage tracks. In this case the tracks of modified material feature a decrease of refractive index (*i.e.* cladding), whereas the material in between the tracks has a higher refractive index (*i.e.* core), thus resulting in a Type II waveguide. This kind of waveguides has been achieved in different materials and is explained in detail elsewhere [41–45]. However, not every zinc aluminum phosphate glass

composition is suitable to be processed and simultaneously result in smooth optical modifications and waveguiding operation. Thus, we explore the suitability of the set of samples presented in Table 1 that contain different alumina levels and [O]/[P] ratios.

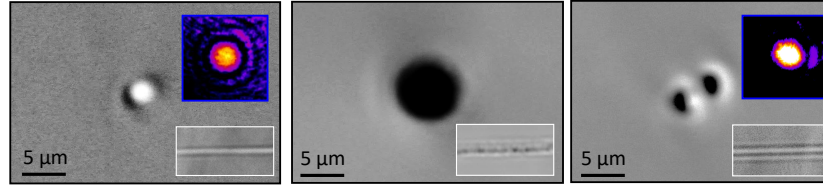


Fig. 2. White light microscopy images of the cross section of a fs-laser machined waveguide (left, $E = 0.5 \mu\text{J}$) and a track of damaged material (center, $E = 2.5 \mu\text{J}$) produced in the sample with a composition of a 5 % Al_2O_3 , 51 % ZnO and 44 % P_2O_5 . Two parallel adjacent tracks of damage (right, $E = 2.0 \mu\text{J}$) are also shown to guide light in the glass sample with a 60 % ZnO and 40 % P_2O_5 . These lines were inscribed using a repetition rate of 1 kHz and a writing speed of $50 \mu\text{m/s}$. The insets show WLM images of the lateral view and the near field profiles of the waveguides at 660 nm. Note that the image size and grey-scale are the same for all the images.

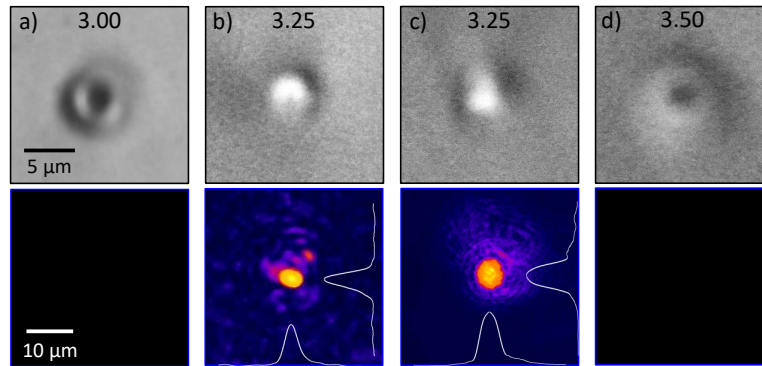


Fig. 3. The top row shows white light microscopy images of the cross section of fs-laser machined lines within glass samples with compositions (a) 30 % ZnO 60 % P_2O_5 10 % Al_2O_3 (b) 42 % ZnO 48 % P_2O_5 10 % Al_2O_3 (c) 51 % ZnO 44 % P_2O_5 5 % Al_2O_3 and (d) 50 % ZnO and 40 % P_2O_5 10 % Al_2O_3 . The [O]/[P] ratio is specified on the WLM images. The lower row shows the near field profiles measured for each line using a CW laser at 660 nm. The laser processing conditions were set the same for the four glass compositions, namely a pulse energy of $0.5 \mu\text{J}$, a repetition rate of 1 kHz and a writing speed of $50 \mu\text{m/s}$.

Fig. 3 shows white light microscopy images of lines inscribed inside glass samples with relevant [O]/[P] ratios, (a) 3.00, (b),(c) 3.25 and (d) 3.50 and different alumina contents. We used the same processing conditions to fabricate these lines, *i.e.* $0.5 \mu\text{J}$, 1 kHz and $50 \mu\text{m/s}$. The lower row illustrates the near field profiles of the guided modes at 660 nm. We empirically find that zinc aluminium phosphate glass compositions with an [O]/[P] ratio of 3.25 are confirmed to be suitable candidates for waveguide inscription. The micrographs and near field profiles illustrate that waveguiding is not achieved in glasses with $3.00 \leq [\text{O}]/[\text{P}] < 3.25$ and $3.25 < [\text{O}]/[\text{P}] \leq 3.50$. Those compositions present a negative change in the refractive index within the fs-laser processed region, thus being unable to guide light. Three of the polyphosphate glasses, with an [O]/[P] ratio equal to 3.25, show a positive change in the refractive index, irrespective of their alumina content. We characterized the laser-induced optical change (see Table 1) and

the numerical aperture of the waveguides by recording the far field profile at a given distance, resulting in a refractive index change of $\Delta n = 3 \times 10^{-4}$ (*i.e.* core), whereas $n_g = 1.576$ is the refractive index of the unmodified glass (*i.e.* cladding). We measured an insertion loss of 6.4 dB. These results are summarized in Table 1 and evidence a clear influence of the glass composition in the suitability for waveguide fabrication, where the ternary phosphate glasses present the same [O]/[P] ratio trend our group reported for binary phosphate glasses [32, 36–38]. The ternary glasses, suitable for waveguide inscription, also present a slight increase of the damage threshold (*i.e.* upper limit for waveguide machining) for decreasing contents of alumina (see Table 1).

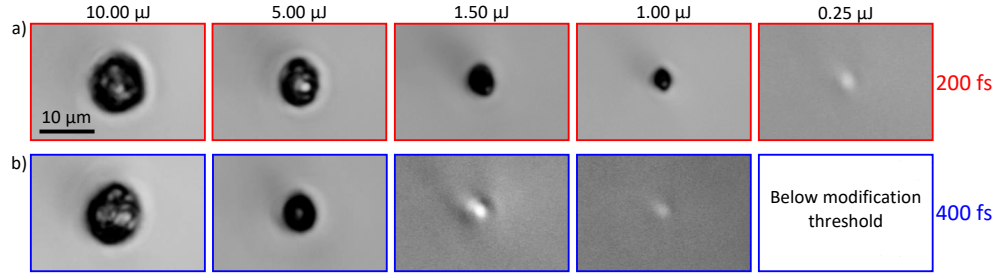


Fig. 4. WLM images of the cross section of fs-laser machined lines of modified glass using a variety of energies and 200 fs (a) and 400 fs (b) laser pulses inside sample 42 % ZnO 48 % P_2O_5 10 % Al_2O_3 . The processing speed was kept constant to be 50 $\mu m/s$ while using a repetition rate of 1 kHz.

In order to reduce undesired non-linear propagation effects and premature laser-induced damage we also tested the fabrication of waveguides using stretched laser pulses. Fig. 4 presents white light microscopy images of laser-written lines inside sample 42 % ZnO 48 % P_2O_5 10 % Al_2O_3 (*i.e.* [O]/[P] = 3.25) using several energies (0.25–10.00 μJ) and two pulse durations (a) 200 fs and (b) 400 fs. We observe that the pulse duration has two important effects in the range of laser energies where good waveguides can be produced. First, the energy threshold linked to smooth modifications increases from $E_{th}^{200 fs} = 0.25 \mu J$ to $E_{th}^{400 fs} = 0.50 \mu J$ when using 400 fs laser pulses, see for instance Fig. 4 (a) and (b) at 1 μJ . The reason for such threshold increment roots on the inherent non-linearity of the laser energy deposition mechanisms in glasses [46, 47]. In this context, a fs-laser pulse focused inside glass generates a dense electron plasma, whose population rate equations are governed by multiphoton ionization and avalanche ionization, *i.e.* the former depends on the k^{th} power of the intensity, where $k = [(U_g/\hbar\omega_L) + 1]$ [48, 49]. The damage threshold is closely related to the number of laser photons used to excite electrons (n_e) as well as to the laser intensity ($dn_e/dt \propto I(t)^k$), which is a measure of the laser energy deposited into the glass. The second observation is an increase of the damage threshold (E_{th}^d) or equivalently a simultaneous shift and stretching in the processing regime where good waveguides are obtained *i.e.* $0.25 \mu J \leq E_{200 fs}^{wg} \leq 0.50 \mu J$ and $0.50 \mu J \leq E_{400 fs}^{wg} \leq 2.50 \mu J$. This widening on the waveguide fabrication regime facilitates the experiment to further test the validity of glass compositions. We also observe such an effect in glasses with other compositions including i) 60 % ZnO 40 % P_2O_5 and ii) 51 % ZnO 44 % P_2O_5 5 % Al_2O_3 . In this way, we confirm that only compositions that have an [O]/[P] ratio equal to 3.25 are feasible candidates to inscribe good quality waveguides thus finding that the reduction of non-linear effects does not facilitate waveguide inscription in glasses with an [O]/[P] \neq 3.25. Moreover, as long as the [O]/[P] ratio remains equal to 3.25 the content of alumina does not influence the waveguide inscription process up to a 10 % Al_2O_3 .

3.2. Raman spectroscopy characterization

The glass samples were investigated with confocal Raman spectroscopy both before and after laser modification in order to elucidate the induced structural changes. We used an excitation CW laser at 473 nm to scan the cross-section of the input facet of the modifications, recording the individual spectrum for each location by using a lens objective (NA = 0.42, 50x) [33, 50, 51]. Fig. 5 shows the bulk Raman spectra from unmodified glass samples with varying levels of alumina and a systematically increasing [O]/[P] ratio. The spectra have been normalized to the maximum value of the band centered at 400 cm^{-1} so we can easily compare the relative intensities of representative Raman bands after fs-laser modification (*i.e.* 702 cm^{-1} and 1209 cm^{-1}). A description of the structure and properties of zinc aluminophosphate glasses linked with their Raman spectra is given below, references [52, 53] provide further details.

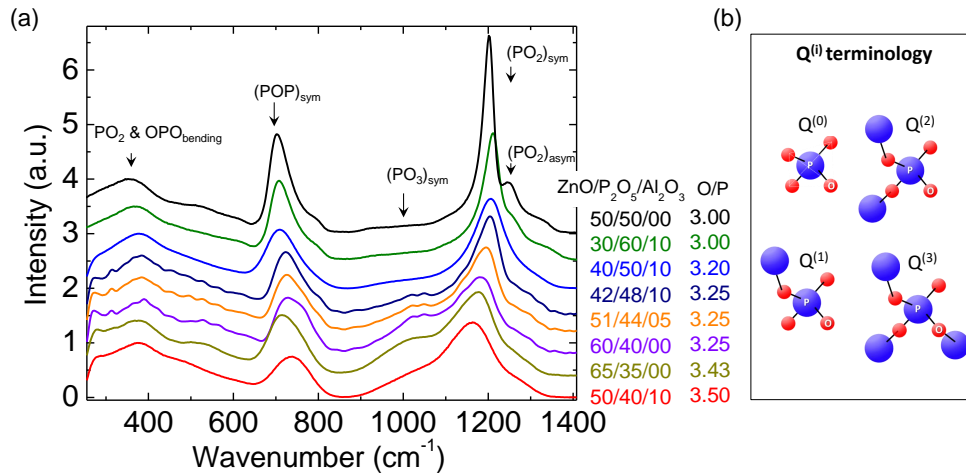


Fig. 5. (a) Raman spectra of the unmodified set of glasses along with composition and [O]/[P] ratios. The main Raman bands and their relation with the vibrational modes are indicated. (b) $Q^{(i)}$ terminology cartoons.

The spectra presented in Fig. 5 (a) indicate five bands that are caused by vibrations associated with the metaphosphate and polyphosphate glass matrix. The structure of the glass matrix can be described as a network of phosphate tetrahedra that are connected together via corner shared oxygen atoms, forming an interconnected network of long *polymer like* phosphate chains, see references [36, 37, 53] for a detailed analysis. The elementary units are based on phosphate tetrahedra, which we illustrate with the cartoons in Fig. 5(b), whose oxygen atoms can be non-bridging atoms. These are categorised using $Q^{(i)}$ terminology, where i denotes the number of bridging oxygens per tetrahedron. The broad Raman signal in the low wavenumber region is due to complex internal deformation bending modes of phosphate chains, both in chain PO_2 and O-P-O bending (350 cm^{-1} bending mode of phosphate polyhedra with zinc modifier and 575 cm^{-1} bend mode related to zinc phosphate network or ZnO_4). The bands around 702 cm^{-1} and 940 cm^{-1} present the symmetric and asymmetric stretching modes of bridging oxygen between two $Q^{(2)}$ tetrahedra, $(\text{POP})_{\text{sym}}$ and $(\text{POP})_{\text{asym}}$, respectively. The band at 1000 cm^{-1} is linked to the symmetric stretching modes, $(\text{PO}_3)_{\text{sym}}$, of terminating P-O bonds that link to one other tetrahedron ($Q^{(1)}$). The band near 1209 cm^{-1} is related to the symmetric stretching associated with the O-P-O non-bridging oxygens on $Q^{(2)}$ phosphate tetrahedra, $(\text{PO}_2)_{\text{sym}}$. The 1300 cm^{-1} peak on the shoulder of the 1209 cm^{-1} band is the asymmetric stretching of O-P-O non-bridging oxygens, $(\text{PO}_2)_{\text{asym}}$. The spectra measured in the metaphosphate regime ($[\text{O}]/[\text{P}] = 3.0$) illustrate glass networks based on $Q^{(2)}$ tetrahedra indicating the formation of long metaphosphate chains.

As the $[O]/[P]$ ratio increases the Raman spectra reveal that $Q^{(2)}$ tetrahedra, which form long chains in metaphosphate glasses, are substituted by $Q^{(1)}$ tetrahedra. Those $Q^{(1)}$ substitutes terminate shorter chains in the polyphosphate regime ($3.0 < [O]/[P] \leq 3.5$).

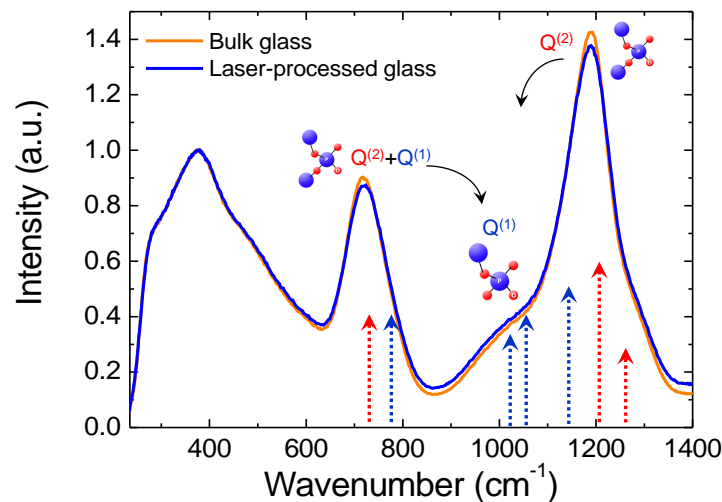


Fig. 6. Raman spectra of unprocessed (orange) and laser-processed (blue) ternary zinc aluminum phosphate glass sample with a 10 % Al_2O_3 , 45 % ZnO and 45 % P_2O_5 . The arrows show the position for different relevant peaks associated to different vibrational modes, *i.e.* blue $Q^{(1)}$ and red $Q^{(2)}$. The schematics near the Raman bands indicate the depolymerization of $Q^{(2)}$ tetrahedra into $Q^{(1)}$. The track of damage studied here was produced by using a laser pulse energy of 5 μJ , a repetition rate of 1 kHz and a writing speed of 50 $\mu m/s$.

Fig. 6 shows two Raman spectra obtained for laser-modified (blue line) and unmodified (orange line) glass with composition 10 % Al_2O_3 , 45 % ZnO and 45 % P_2O_5 . The bands centered at 702 cm^{-1} ($(POP)_{sym}$) and 1209 cm^{-1} ($(PO_2)_{sym}$), which are associated to $Q^{(2)}$ tetrahedra, decrease for the laser processed glass. While $Q^{(2)}$ peaks decrease, the Raman bands near 1000 cm^{-1} , linked to $Q^{(1)}$ tetrahedra, slightly increase. These spectral changes are indicative of structural depolymerization (*i.e.* $Q^{(2)}$ transforms into $Q^{(1)}$). In addition the Raman peak at 1209 cm^{-1} also shows a subtle shift towards lower wavenumbers that indicates a glass network expansion and consequently a decrease of the local refractive index, as previously reported for binary phosphate glasses [36,37].

We have mapped the laser-induced depolymerization for inscribed lines inside three different glasses. Fig. 7 shows microscopy images (a) along with Raman maps (b),(c) of tracks inscribed inside glasses with 3.25 (first three columns) and 3.33 (fourth column) $[O]/[P]$ ratios. The results in the first two columns clearly show that there are no significant Raman changes for the samples that display waveguiding. In particular, we do not find evidence of a positive Raman peak shift that would point to a network contraction, a material densification and thus a positive refractive index change. In contrast, tracks of damage feature measurable changes through Raman analysis, as shown in Fig. 7 (b) and (c) (*i.e.* last two columns). The relative change in the Raman intensities in Fig. 7 (b) and the peak shifts in Fig. 7 (c) reveal a depolymerization of the glass network and a network expansion, respectively. This expansion leads to a decrease in the local density and presumably to a decrease in the refractive index thus not allowing for guiding to occur.

Overall, these results concur with our earlier work on binary phosphate glasses in that no positive Raman peak shift was detected even though the glass clearly shows guiding [36] and thus

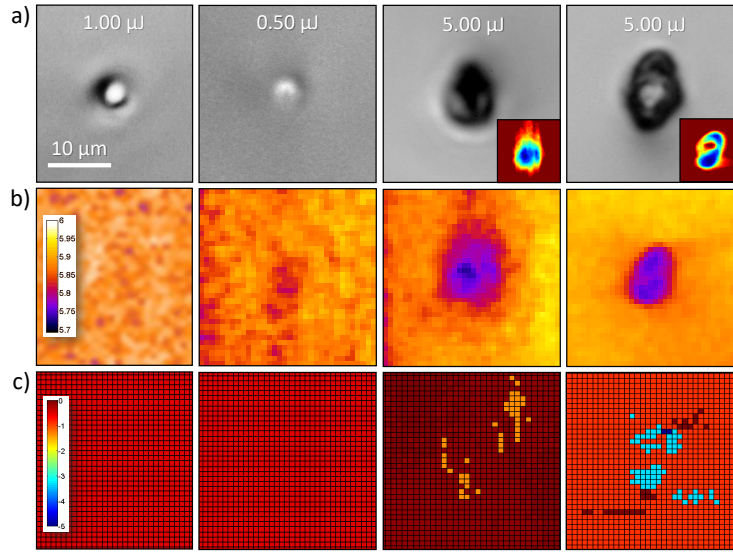


Fig. 7. Optical microscopy (a) and Raman spectral microscopy characterization (b)-(c) of laser fabricated lines inside zinc aluminum phosphate glasses. The images in the first column correspond to sample 60 % ZnO 40 % P₂O₅ with an [O]/[P] ratio of 3.25, the second and third columns correspond to sample 42 % ZnO 48 % P₂O₅ 10 % Al₂O₃ with an [O]/[P] ratio of 3.25, the fourth column correspond to sample 45 % ZnO 45 % P₂O₅ 10 % Al₂O₃ with an [O]/[P] ratio of 3.33. The false color maps in (b) present the relative amplitude change (a.u.) between 1209 cm⁻¹/1000 cm⁻¹ Raman peaks. The false color maps in (c) illustrate the Shift of the 1209 cm⁻¹ Raman peak (δcm⁻¹). Note that the whole set of images share the same lateral size. The machined lines studied here were produced by using various laser pulse energies (specified on the optical micrographs), a repetition rate of 1 kHz and a writing speed of 50 μm/s.

must have undergone a change in index, which is normally associated with a change in the glass network structure. A laser-induced modification of the material polarizability that is mediated by an increase of the Q⁽¹⁾ tetrahedra [34] could potentially explain this subtle increase. However, we do not observe any substantial increase of the Q⁽¹⁾ bands when studying the laser-inscribed waveguides with Raman spectroscopy.

3.3. Laser-fabricated waveguide Bragg gratings in zinc magnesium phosphate glasses

We have so far studied the fabrication of optical waveguides inside binary and ternary zinc aluminum phosphate glasses by testing the role of the glass composition and the laser-induced structural changes. Here, we investigate the use of waveguide Bragg grating (WBG) inscription inside a ternary zinc magnesium phosphate glass (see glass preparation) to create optical filters/mirrors with different spectral characteristics. Typically WBGs are inscribed inside optical fibers to produce fiber Bragg gratings (FBGs) for telecom purposes [54] and also inside bulk material to generate volume Bragg gratings (VBGs) [40,55]. Fig. 8 (a) shows a schematic of an optical filter and selective mirror based on a WBG. The cartoon illustrates a periodic refractive index track that forms the Bragg grating. The principle of operation in a WBG roots on the interaction of the light with the periodic refractive index, which selectively reflects and transmits light based on the interference of waves. The condition for light with a particular wavelength to be reflected is $\lambda_{WBG} = 2n_e\Lambda$, where Λ stands for the spatial period of the structure and $n_e = 1.55$ is the refractive index of the glass. Based on this relation, we can precisely design the

performance of the laser-fabricated filter by simply calculating the writing speed that will result in a certain spatial period Λ , *i.e.* writing speed = $\Lambda \times$ repetition rate.

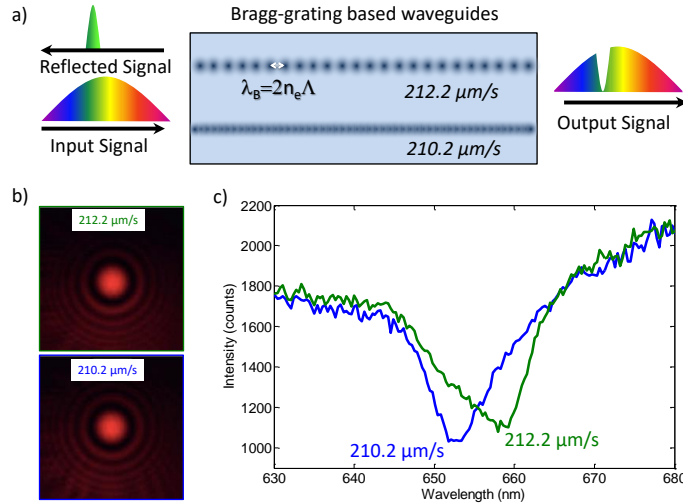


Fig. 8. (a) Waveguide Bragg grating schematic. (b) output modes of the WBGs inscribed using two processing speeds inside glass sample with composition 28 % ZnO, 28 % MgO, 42 % P₂O₅, 1.3 % Yb₂O₃ and 0.7 % Yb₂O₃. (c) Transmission spectra of the laser-fabricated WBGs filters. The filters inscribed using writing speeds of 210.2 $\mu\text{m/s}$ and 212.2 $\mu\text{m/s}$ have transmission loss of -2.1 dB and -1.9 dB, respectively.

During fs-laser direct-write, we then controlled the spatial periodicity of the filter by tuning the processing speed while maintaining the repetition rate (1 kHz) and laser energy (600 nJ). In this way, we wrote two WBGs using a single pass procedure and two slightly different speeds, *i.e.* 210.2 $\mu\text{m/s}$ and 212.2 $\mu\text{m/s}$, corresponding to $\lambda_{WBG} = 652$ and 658 nm, respectively. Fig. 8 (b) shows output modes of the waveguides when coupling a CW laser at 660 nm, thus confirming we successfully inscribed the waveguides. The far field numerical aperture provides an estimate of the refractive index change of $\approx 10^{-4}$.

Then, we determined the spectral features of the waveguide Bragg gratings by measuring the relative transmission using a white light source (Ocean Optics, DH-2000). We used an optical fiber (Ocean Optics, P100-2 VIS/NIR) to couple the light directly to the input of the waveguides and collect the transmitted light using another fiber (Ocean Optics, P8-2-SMA). Both fibers and the sample were carefully aligned and positioned using micrometer driven translation stages and immersion oil (Cargille Type-B). Fig. 8 (c) depicts the transmitted spectra through the WBG. The dips in transmission are centered at 652 nm and 658 nm, respectively for the 210.2 $\mu\text{m/s}$ and 212.2 $\mu\text{m/s}$ processing speeds, in excellent agreement with the predicted values.

4. Conclusion

In this work we studied the suitability of ternary phosphate glasses for femtosecond laser micromachining of a variety of devices. We tested ten zinc aluminium phosphate glasses with increasing [O]/[P] ratios for fabricating optical waveguides and an Er/Yb doped zinc magnesium phosphate glass for inscribing waveguides Bragg gratings using fs-laser pulses. We were able to produce optical waveguides inside zinc aluminium phosphate glasses with an [O]/[P] ratio equal to 3.25 independently of the aluminium content, resulting in a refractive index change of $3 \cdot 10^{-4}$. We found that longer pulse durations lead to a widening in the range of processing energies that result in waveguiding operation. Using confocal Raman spectroscopy we correlated femtosecond

laser-induced damage to an apparent depolymerization of the glass network, where $Q^{(2)}$ species decrease while $Q^{(1)}$ and $Q^{(0)}$ increase. Finally we illustrate the fs-laser fabrication and design of filters and mirrors inside a ternary zinc magnesium phosphate glass with selective spectral features based on waveguide Bragg gratings.

Funding

National Science Foundation (DMR 1206979 and DMR 1207520).

Acknowledgments

We acknowledge fruitful discussions with Luke Fletcher and Charmayne Smith. We are also grateful to Vladimir Semenov and Nikolay Skovorodnikov for support with the laser experiments. We thank Gordon Soekland for assistance on grinding and polishing procedures.

References

1. A. Vogel and V. Venugopalan, "Mechanisms of pulsed laser ablation of biological tissues," *Chem. Rev.* **103**, 577–644 (2003).
2. R. R. Gattass and E. Mazur, "Femtosecond laser micromachining in transparent materials," *Nat. Photonics* **2**, 219 (2008).
3. C. Wagner and N. Harned, "Euv lithography: Lithography gets extreme," *Nat. Photonics* **4**, 24 (2010).
4. T. T. Fernandez, S. M. Eaton, G. D. Valle, R. M. Vazquez, M. Irannejad, G. Jose, A. Jha, G. Cerullo, R. Osellame, and P. Laporta, "Femtosecond laser written optical waveguide amplifier in phospho-tellurite glass," *Opt. Express* **18**, 20289–20297 (2010).
5. B. Sotillo, V. Bharadwaj, J. Hadden, M. Sakakura, A. Chiappini, T. T. Fernandez, S. Longhi, O. Jedrkiewicz, Y. Shimotsuma, L. Criante *et al.*, "Diamond photonics platform enabled by femtosecond laser writing," *Sci. Reports* **6**, 35566 (2016).
6. E. N. Glezer and E. Mazur, "Ultrafast-laser driven micro-explosions in transparent materials," *Appl. Phys. Lett.* **71**, 882–884 (1997).
7. C. Hnatovsky, R. Taylor, E. Simova, P. Rajeev, D. Rayner, V. Bhardwaj, and P. Corkum, "Fabrication of microchannels in glass using focused femtosecond laser radiation and selective chemical etching," *Appl. Phys. A* **84**, 47–61 (2006).
8. C. B. Schaffer, A. Brodeur, and E. Mazur, "Laser-induced breakdown and damage in bulk transparent materials induced by tightly focused femtosecond laser pulses," *Meas. Sci. Technol.* **12**, 1784 (2001).
9. G. D. Marshall, A. Politi, J. C. Matthews, P. Dekker, M. Ams, M. J. Withford, and J. L. O'Brien, "Laser written waveguide photonic quantum circuits," *Opt. Express* **17**, 12546–12554 (2009).
10. S. Taccheo, G. Della Valle, R. Osellame, G. Cerullo, N. Chiodo, P. Laporta, O. Svelto, A. Killi, U. Morgner, M. Lederer *et al.*, "Er: Yb-doped waveguide laser fabricated by femtosecond laser pulses," *Opt. Lett.* **29**, 2626–2628 (2004).
11. Q. Sun, H. Jiang, Y. Liu, Y. Zhou, H. Yang, and Q. Gong, "Effect of spherical aberration on the propagation of a tightly focused femtosecond laser pulse inside fused silica," *J. Opt. A: Pure Appl. Opt.* **7**, 655 (2005).
12. A. Marcinkevičius, V. Mizeikis, S. Juodkazis, S. Matsuo, and H. Misawa, "Effect of refractive index-mismatch on laser microfabrication in silica glass," *Appl. Phys. A* **76**, 257–260 (2003).
13. K. M. Davis, K. Miura, N. Sugimoto, and K. Hirao, "Writing waveguides in glass with a femtosecond laser," *Opt. Lett.* **21**, 1729–1731 (1996).
14. K. Miura, J. Qiu, H. Inouye, T. Mitsuyu, and K. Hirao, "Photowritten optical waveguides in various glasses with ultrashort pulse laser," *Appl. Phys. Lett.* **71**, 3329–3331 (1997).
15. K. Hirao and K. Miura, "Writing waveguides and gratings in silica and related materials by a femtosecond laser," *J. Non-Crystalline Solids* **239**, 91–95 (1998).
16. N. Psaila, R. Thomson, H. Bookey, A. Kar, N. Chiodo, R. Osellame, G. Cerullo, A. Jha, and S. Shen, "Er: Yb-doped oxyfluoride silicate glass waveguide amplifier fabricated using femtosecond laser inscription," *Appl. Phys. Lett.* **90**, 131102 (2007).
17. A. M. Streltsov and N. F. Borrelli, "Study of femtosecond-laser-written waveguides in glasses," *JOSA B* **19**, 2496–2504 (2002).
18. J. Hernandez-Rueda, J. Clarijs, D. van Oosten, and D. M. Krol, "The influence of femtosecond laser wavelength on waveguide fabrication inside fused silica," *Appl. Phys. Lett.* **110**, 161109 (2017).
19. J. J. Witcher, J. Hernandez-Rueda, and D. M. Krol, "Fs-laser processing of glass: Plasma dynamics and spectroscopy," *Int. J. Appl. Glass Sci.* **6**, 220–228 (2015).
20. M. Ams, G. Marshall, D. Spence, and M. Withford, "Slit beam shaping method for femtosecond laser direct-write fabrication of symmetric waveguides in bulk glasses," *Opt. Express* **13**, 5676–5681 (2005).

21. T. T. Fernandez, B. Sotillo, J. d. Hoyo, J. Valleś, R. M. Vázquez, P. Fernandez, and J. Solis, "Dual regimes of ion migration in high repetition rate femtosecond laser inscribed waveguides," *IEEE Photonics Technol. Lett.* **27**, 1068–1071 (2015).
22. L. Englert, B. Rethfeld, L. Haag, M. Wollenhaupt, C. Sarpe-Tudoran, and T. Baumert, "Control of ionization processes in high band gap materials via tailored femtosecond pulses," *Opt. Express* **15**, 17855–17862 (2007).
23. P. Salter, A. Jesacher, J. Spring, B. Metcalf, N. Thomas-Peter, R. D. Simmonds, N. Langford, I. Walmsley, and M. J. Booth, "Adaptive slit beam shaping for direct laser written waveguides," *Opt. letters* **37**, 470–472 (2012).
24. J. Hernandez-Rueda, J. Siegel, M. Galvan-Sosa, A. R. de la Cruz, and J. Solis, "Surface structuring of fused silica with asymmetric femtosecond laser pulse bursts," *JOSA B* **30**, 1352–1356 (2013).
25. M. Sakakura, T. Kurita, M. Shimizu, K. Yoshimura, Y. Shimotsuna, N. Fukuda, K. Hirao, and K. Miura, "Shape control of elemental distributions inside a glass by simultaneous femtosecond laser irradiation at multiple spots," *Opt. Lett.* **38**, 4939–4942 (2013).
26. J. Hernandez-Rueda, J. Siegel, M. Galvan-Sosa, A. R. de la Cruz, M. Garcia-Lechuga, and J. Solis, "Controlling ablation mechanisms in sapphire by tuning the temporal shape of femtosecond laser pulses," *J. Opt. Soc. Am. B* **32**, 150–156 (2015).
27. S. M. Eaton, H. Zhang, P. R. Herman, F. Yoshino, L. Shah, J. Bovatsek, and A. Y. Arai, "Heat accumulation effects in femtosecond laser-written waveguides with variable repetition rate," *Opt. Express* **13**, 4708–4716 (2005).
28. R. Osellame, N. Chiodo, G. D. Valle, G. Cerullo, R. Ramponi, P. Laporta, A. Killi, U. Morgner, and O. Svelto, "Waveguide lasers in the c-band fabricated by laser inscription with a compact femtosecond oscillator," *IEEE J. Sel. Top. Quantum Electron.* **12**, 277–285 (2006).
29. T. Fernandez, M. Sakakura, S. Eaton, B. Sotillo, J. Siegel, J. Solis, Y. Shimotsuna, and K. Miura, "Bespoke photonic devices using ultrafast laser driven ion migration in glasses," *Prog. Mater. Sci.* **94**, 68 – 113 (2018).
30. A. Jha, B. Richards, G. Jose, T. Teddy-Fernandez, P. Joshi, X. Jiang, and J. Lousteau, "Rare-earth ion doped teo2 and geo2 glasses as laser materials," *Prog. Mater. Sci.* **57**, 1426–1491 (2012).
31. T. T. Fernandez, G. D. Valle, R. Osellame, G. Jose, N. Chiodo, A. Jha, and P. Laporta, "Active waveguides written by femtosecond laser irradiation in an erbium-doped phospho-tellurite glass," *Opt. Express* **16**, 15198–15205 (2008).
32. L. B. Fletcher, J. J. Witcher, N. Troy, R. K. Brow, and D. M. Krol, "Single-pass waveguide amplifiers in er-yb doped zinc polyphosphate glass fabricated with femtosecond laser pulses," *Opt. letters* **37**, 1148–1150 (2012).
33. J. W. Chan, T. R. Huser, S. H. Risbud, J. S. Hayden, and D. M. Krol, "Waveguide fabrication in phosphate glasses using femtosecond laser pulses," *Appl. Phys. Lett.* **82**, 2371–2373 (2003).
34. D. J. Little, M. Ams, P. Dekker, G. D. Marshall, and M. J. Withford, "Mechanism of femtosecond-laser induced refractive index change in phosphate glass under a low repetition-rate regime," *J. Appl. Phys.* **108**, 033110 (2010).
35. Y. Duan, P. Dekker, M. Ams, G. Palmer, and M. J. Withford, "Time dependent study of femtosecond laser written waveguide lasers in yb-doped silicate and phosphate glass," *Opt. Mater. Express* **5**, 416–422 (2015).
36. L. B. Fletcher, J. J. Witcher, N. Troy, S. T. Reis, R. K. Brow, and D. M. Krol, "Direct femtosecond laser waveguide writing inside zinc phosphate glass," *Opt. Express* **19**, 7929–7936 (2011).
37. L. B. Fletcher, J. J. Witcher, N. Troy, S. T. Reis, R. K. Brow, R. M. Vazquez, R. Osellame, and D. M. Krol, "Femtosecond laser writing of waveguides in zinc phosphate glasses," *Opt. Mater. Express* **1**, 845–855 (2011).
38. L. B. Fletcher, J. J. Witcher, N. Troy, S. T. Reis, R. K. Brow, and D. M. Krol, "Effects of rare-earth doping on femtosecond laser waveguide writing in zinc polyphosphate glass," *J. Appl. Phys.* **112**, 023109 (2012).
39. D. Krol, "Femtosecond laser modification of glass," *J. Non-Crystalline Solids* **354**, 416–424 (2008).
40. G. D. Marshall, M. Ams, and M. J. Withford, "Direct laser written waveguide-Bragg gratings in bulk fused silica," *Opt. Lett.* **31**, 2690–2691 (2006).
41. D. G. Lancaster, S. Gross, H. Ebendorff-Heidepriem, K. Kuan, T. M. Monro, M. Ams, A. Fuerbach, and M. J. Withford, "Fifty percent internal slope efficiency femtosecond direct-written tm3+ :zblan waveguide laser," *Opt. Lett.* **36**, 1587–1589 (2011).
42. A. G. Okhrimchuk, A. V. Shestakov, I. Khrushchev, and J. Mitchell, "Depressed cladding, buried waveguide laser formed in a yag:nd3+ crystal by femtosecond laser writing," *Opt. Lett.* **30**, 2248–2250 (2005).
43. J. Burghoff, S. Nolte, and A. Tünnermann, "Origins of waveguiding in femtosecond laser-structured linbo3," *Appl. Phys. A* **89**, 127–132 (2007).
44. T. Gorelik, M. Will, S. Nolte, A. Tuennermann, and U. Glatzel, "Transmission electron microscopy studies of femtosecond laser induced modifications in quartz," *Appl. Phys. A* **76**, 309–311 (2003).
45. A. Ródenas, G. A. Torchia, G. Lifante, E. Cantelar, J. Lamela, F. Jaque, L. Roso, and D. Jaque, "Refractive index change mechanisms in femtosecond laser written ceramic nd:yag waveguides: micro-spectroscopy experiments and beam propagation calculations," *Appl. Phys. B* **95**, 85–96 (2009).
46. J. Hernandez-Rueda, D. Puerto, J. Siegel, M. Galvan-Sosa, and J. Solis, "Plasma dynamics and structural modifications induced by femtosecond laser pulses in quartz," *Appl. Surf. Sci.* **258**, 9389–9393 (2012).
47. J. Hernandez-Rueda, N. Goñe, J. Siegel, M. Soccio, B. Zielinski, C. Sarpe, M. Wollenhaupt, T. A. Ezquerro, T. Baumert, and J. Solis, "Nanofabrication of tailored surface structures in dielectrics using temporally shaped femtosecond-laser pulses," *ACS Appl. Mater. & Interfaces* **7**, 6613–6619 (2015).
48. B. Rethfeld, K. Sokolowski-Tinten, D. von der Linde, and S. Anisimov, "Timescales in the response of materials to femtosecond laser excitation," *Appl. Phys. A* **79**, 767–769 (2004).
49. B. Rethfeld, "Unified model for the free-electron avalanche in laser-irradiated dielectrics," *Phys. Rev. Lett.* **92**, 187401

- (2004).
50. W. J. Reichman, D. M. Krol, L. Shah, F. Yoshino, A. Arai, S. M. Eaton, and P. R. Herman, "A spectroscopic comparison of femtosecond-laser-modified fused silica using kilohertz and megahertz laser systems," *J. Appl. Phys.* **99**, 123112 (2006).
 51. J. W. Chan, T. Huser, J. S. Hayden, S. H. Risbud, and D. M. Krol, "Fluorescence spectroscopy of color centers generated in phosphate glasses after exposure to femtosecond laser pulses," *J. Am. Ceram. Soc.* **85**, 1037–1040 (2002).
 52. R. K. Brow, D. R. Tallant, S. T. Myers, and C. C. Phifer, "The short-range structure of zinc polyphosphate glass," *J. Non-Crystalline Solids* **191**, 45–55 (1995).
 53. C. E. Smith, R. K. Brow, L. Montagne, and B. Revel, "The structure and properties of zinc aluminophosphate glasses," *J. Non-Crystalline Solids* **386**, 105 – 114 (2014).
 54. K. Hill, Y. Fujii, D. C. Johnson, and B. Kawasaki, "Photosensitivity in optical fiber waveguides: Application to reflection filter fabrication," *Appl. Phys. Lett.* **32**, 647–649 (1978).
 55. O. M. Efimov, L. B. Glebov, L. N. Glebova, K. C. Richardson, and V. I. Smirnov, "High-efficiency Bragg gratings in photothermorefractive glass," *Appl. Opt.* **38**, 619–627 (1999).